Impaired development of neocortical circuits contributes to the neurological alterations in *DYRK1A* haploinsufficiency syndrome

Juan Arranz, Elisa Balducci, Kristina Arató, Gentzane Sánchez-Elexpuru, Sònia Najas, Alberto Parras, Elena Rebollo, Isabel Pijuan, Ionas Erb, Gaetano Verde, Ignasi Sahun, Maria J. Barallobre, José J. Lucas, Marina P. Sánchez, Susana de la Luna, Maria L. Arbonés

Supplementary Materials and Methods

Western blots

Samples were resolved by SDS-PAGE and the proteins were transferred onto nitrocellulose membranes (Amersham Protran). The membranes were blocked for 30 min at room temperature with 10% skimmed milk (Sigma) diluted in 10 mM Tris-HCl [pH 7.5], 100 mM NaCl (TBS) plus 0.1% Tween-20 (TBS-T), and then incubated overnight at 4ºC with the primary antibodies (Supplementary Table 3) diluted in 5% skimmed milk in TBS-T. After several washes, the membranes were incubated for 45 min at room temperature with horseradish peroxidase-conjugated secondary antibodies (DaKo) diluted in 5% skimmed milk in TBS-T. Antibody binding was detected by enhanced chemiluminiscence (Western Lightning Plus ECL, Perkin Elmer), which was analyzed on a LAS-3000 image analyzer (Fuji PhotoFilm). The antibody signal was quantified with the ImageQuant software. For relative protein accumulation, total cell extracts were used by resuspending the cell pellets in SDS loading buffer. For quantification, the signal of the HA-antibody was corrected with that of the GFP-antibody in co-transfections with pEGFP-C1 (Fig. 1E).

Microarray experiments

The experimental set up is depicted in Supplementary Fig. 6A. Total RNA was prepared from the cerebral cortex of P0 and P7 mice, obtained from two litters (*Dyrk1a*$^{+/+}$, n=4; *Dyrk1a*$^{+/-}$, n=4). Double stranded cDNA was synthesized from 100 ng RNA using the Two Cycle cDNA Synthesis Kit (Affymetrix), according to the manufacturer's instructions. After cRNA purification and fragmentation, the cRNA quality was checked (3'/5' ratio of probe sets <1.5, for *Gapdh* and *Actb* probes). The fragmented cRNA (15 μg) was added to the hybridization mix and used to fill the Affymetrix Mouse GeneChip 430 2.0 Array cartridge (over 39,000 mouse genes). The arrays were hybridized at 60ºC for 16 h with rotation in the Affymetrix GeneChip

Hyb Oven 640, washed and marked with streptavidin R-phycoerythrin following the Affymetrix protocol. After washing, the arrays were scanned in an Agilent G3000 GeneArray Scanner and the images were processed with Microarray Analysis Suite 5.0 (Affymetrix). Raw values obtained from the .CEL files were pre-processed using the Robust Multiarray Averaging Method (Irizarry et al., 2003), and the resulting normalized values were used for all subsequent analyses. The data were first subjected to non-specific filtering to remove low signal genes (those whose expression was below the third quartile of all expression values) and low variability genes (those whose standard deviation of the expression was below the third quartile of all standard deviations). All the statistical analyses were performed with the "R" statistical software and the libraries developed for microarray data analysis using the Bioconductor Project (www.bioconductor.org). Probes with an adjusted *p*-value ≤ 0.05 that mapped to a known mouse gene were selected for the results shown in Fig. 5 (Supplementary Dataset 1).

RT-qPCR

The cDNA was synthesized from 1 μg of total RNA using Superscript II retrotranscriptase (Invitrogen) and random hexamers. Real-time qPCR was carried out on the Lightcycler 480 platform (Roche), using the SYBR Green I Master kit (Roche) and cDNA diluted 1:10, mixing the reagents according to the manufacturer's recommendations. In general, the PCR conditions were: one cycle 95°C 5 min; 45 cycles 95°C 10 sec, 60°C 10 s and 72°C 10 s; one cycle 95°C 5 sec and 65°C 1 min. Primers for RT-qPCR, were designed using the "Primer3" tool (frodo.wi.mit.edu/cgi-bin/primer3/primer3) to obtain 80-200 bp amplicons and optimal annealing temperatures between 59 and 61ºC for each primer pair (Supplementary Table 4). We used *Ppia* as a reference gene for data normalization. Each sample was assayed in triplicate and the Ct (threshold cycle) was calculated using the relative

quantification of the second derivative maximum method with the Lightcycler 480 1.2 software (Roche).

For qPCR experiments on a Low Density array (LDA, Applied Biosystem), cDNA was synthesized from 0.5 μg of total RNA using MultiScribe retrotranscriptase and using random primers (High Capacity cDNA Reverse Transcription Kit, Applied Biosystem), according to the manufacturer's recommendations. For quantitative analysis, the cDNAs were diluted 1:10 in H_2O, added to TaqMan® Universal PCR Master Mix (Applied Biosystem) in a 1:1 ratio and loaded onto the LDA, pre-loaded with the selected TaqMan® Gene Expression Assays (Supplementary Table 5). The TaqMan Array was run on the 7900HT system (Applied Biosystem) following the manufacturer's instructions, and the data were analyzed with the SDS software (Applied Biosystem), based on the Pfaffl Method (Pfaffl, 2001). We used *Ppia* and *Actb* as the reference genes for data normalization.

Computational analysis

The differentially expressed genes were selected based on a linear model analysis with empirical Bayes modification for the variance estimates (Smyth, 2004) and the p-values were adjusted using the Benjamini-Hochberg method (Benjamini and Hochberg, 1995). We used hierarchical clustering with Euclidean distances to form the groups of differentially expressed genes and the heat maps to visualize them. The annotation of the Affymetrix dataset was done with bioDBnet (biodbnet-abcc.ncifcrf.gov: (Mudunuri et al., 2009). The analysis of transcription factor and pathway enrichment was performed using the web server Enrichr (amp.pharm.mssm.edu/Enrichr: (Kuleshov et al., 2016) and its associated visualization tools (Tan et al., 2013). The Ensemble (www.ensembl.org) and NCBI (www.ncbi.nlm.nih.gov) public databases were used to integrate the information regarding gene sequences and functions.

Behavioral Testing

Social interactions

Social interactions between two unfamiliar mice were evaluated using a modification of the reciprocal social interaction test (Lin and Hsueh, 2014). In brief, the subject animal was placed in a standard housed cage (12.5 cm x 17.5 cm x 32.5 cm) with clean bedding and after 5 min of habituation, a male of a different litter but on the same genetic background and age was introduced into the cage. The interactions between the two mice were videotaped during 5 min and the same intruder mouse was used in all tests. We scored the time spent in the social interactions (nose-to-nose sniffing and nose-to-anus sniffing) that were initiated by the subject mouse and the time spent by this mouse performing stereotyped repetitive behaviors (digging and grooming).

Marble-burying

The marble-burying test was performed as described previously (Thomas et al., 2009). In brief, mice were placed in a cage (17.5 cm x 24.5 cm x 42.5 cm) that had 12 black glass marbles (15 mm diameter) evenly spaced in a 2 x 6 grid on top of 5 cm of clean bedding. The mice were videotaped for 20 min, and we scored the number of marbles buried (90% or more covered) and the time spent by the mouse performing stereotyped repetitive behaviors (digging and grooming).

Ultrasonic vocalization (UsV)

UsV was measured in male and female pups at P3, P6, P9 and P12 (4 litters, 17-11 animals each genotype). The dam was removed from a temperature-controlled home cage where the pups remained. The pups were then removed individually from the cage and transported in a dish into a hood equipped with a UsV recorder (Avisoft) where they were recorded for 5 min. Room temperature was maintained at 21ºC and the body temperature was measured with an axillary probe after the 5 min test. The data was analyzed with Avisoft SASLab Pro software.

Immunostaining

To prepare cryotome sections, brains were cryoprotected with 30% sucrose in phosphate-buffered saline (PBS), while for vibratome sections brains were embedded in 4% agarose in H_2O. For immunohistochemistry, cryotome sections (14 μm) were collected on Starfrost precoated slides (Knittel Glasser) and distributed serially. For immunofluorescence, free-floating cryotome and vibratome sections (30-45 μm) were distributed serially in 48-well plates. For bromodeoxyuridine (BrdU) antibodies the sections were treated for 30 min with 2N HCl at 37ºC before blocking (Najas et al., 2015). Immunohistochemistry was performed following the avidin-biotin-peroxidase method (Vectastain ABC kit, Vector Labs, Burlingame, CA, USA) as described previously (Barallobre et al., 2014). In this case, samples were stained with Nissl (0.1% Cresyl violet acetate) to visualized non-immunopositive cells. For immunofluorescence, the sections were blocked for 1 h at room temperature in PBS containing 0.2% Triton-X100 and 10% fetal bovine serum (FBS), and probed for 18 to 96 h at 4ºC with the primary antibodies (Supplementary Table 6) diluted in antibody buffer (PBS with 0.2% Triton-X100 and 5% FBS). For some antibodies, an antigen retrieval treatment was performed before blocking. The sections were then washed and the primary antibodies were detected using Alexa-555 or Alexa-488 conjugated secondary antibodies (1:1000; Life Technologies). Cell nuclei were stained with Hoechst or 4′,6-diamidino-2-phenylindole,(DAPI; Sigma-Aldrich). For antibodies against Gephyrin and Homer, signal amplification was required and thus, after washing the sections they were incubated with the corresponding biotinylated secondary antibody (1:200; Vector Labs), and then with Alexa-488 conjugated streptavidin (Life Technologies). In all cases, the specificity of the immunoreaction was assessed by omitting the primary antibody.

Cell and synapse counts

Wide-field and confocal microscope images were taken from the somatosensory cortex (SSC) and processed using Image J/Fiji (Rasband, W.S., National Institutes of Health, Bethesda, Maryland, USA; imagej.nih.gov/ij).

Cell counts

Cells in postnatal animals were counted in 150 μm wide radial columns ($NeuN^+$ cells), in 350 μm wide radial columns ($Citp2^+$ cells and $Mef2c^+$ cells) or in 500 μm wide radial columns ($BrdU^+$ cells) of the SSC. Labeled cells in adult animals were counted in 150 μm wide radial columns ($NeuN^+/GABA^-$ cells) or in 350 μm wide radial columns ($GABA^+$ cells) of the SSC. All cell counts were obtained blind from images at the same rostro-caudal level of at least 3 sections per animal: from the beginning of the hippocampal commissure to the beginning of the hippocampus in P7 mice, and from bregma -0.22 to bregma -0.94 (Paxinos and Franklin, 2001) in adult mice.

Synapse counts

Tissue samples used for synapse counts where mounted in 2,2'-thiodiethanol adjusted to 1.51 refraction index in order to minimize chromatic shift. Synapses were counted in images from 3 sections at the same rostral-caudal level in each mouse (sections from bregma -0.22 to bregma -0.94). Twenty images (26 μm^2) per hemisphere and layer were analyzed randomly from the SSC layers IV and VI on a Zeiss LSM780 confocal microscope equipped with a Plan Apochromat 63x oil (NA=1.4) objective. 2D confocal sections were acquired by sequential line scanning using the excitation lines 405, 488 and 561 and the respective detection bandwidths 415-491, 490-553 and 568-735. The scanning speed was set at 3.15 μs/pixel and the resolution was adjusted to 50 nm/pixel. All images were acquired under the same parameters to guarantee the signals captured remained within the limits of the dynamic range of detection. A specific algorithm was developed in macro language

to automatically obtain the density of the synapses in all the images (see details in Supplementary Fig. 3).

Supplementary References

Barallobre, M.J., Perier, C., Bove, J., Laguna, A., Delabar, J.M., Vila, M., Arbones, M.L., 2014. DYRK1A promotes dopaminergic neuron survival in the developing brain and in a mouse model of Parkinson's disease. Cell Death Dis 5, e1289.

Benjamini, Y., Hochberg, Y., 1995. Controlling the false discovery rate: a practical and powerful approach to multiple testing. Journal of the Royal Statistical Society. Series B (Methodological) 57, 12.

Bronicki, L.M., Redin, C., Drunat, S., Piton, A., Lyons, M., Passemard, S., Baumann, C., Faivre, L., Thevenon, J., Riviere, J.B.*, et al.*, 2015. Ten new cases further delineate the syndromic intellectual disability phenotype caused by mutations in DYRK1A. Eur J Hum Genet 23, 1482-1487.

Dang, T., Duan, W.Y., Yu, B., Tong, D.L., Cheng, C., Zhang, Y.F., Wu, W., Ye, K., Zhang, W.X., Wu, M.*, et al.*, 2018. Autism-associated Dyrk1a truncation mutants impair neuronal dendritic and spine growth and interfere with postnatal cortical development. Mol Psychiatry 23, 747-758.

De Rubeis, S., He, X., Goldberg, A.P., Poultney, C.S., Samocha, K., Cicek, A.E., Kou, Y., Liu, L., Fromer, M., Walker, S.*, et al.*, 2014. Synaptic, transcriptional and chromatin genes disrupted in autism. Nature 515, 209-215.

Deciphering Developmental Disorders, S., 2015. Large-scale discovery of novel genetic causes of developmental disorders. Nature 519, 223-228.

Evers, J.M., Laskowski, R.A., Bertolli, M., Clayton-Smith, J., Deshpande, C., Eason, J., Elmslie, F., Flinter, F., Gardiner, C., Hurst, J.A.*, et al.*, 2017. Structural analysis of pathogenic mutations in the DYRK1A gene in patients with developmental disorders. Hum Mol Genet 26, 519-526.

Irizarry, R.A., Hobbs, B., Collin, F., Beazer-Barclay, Y.D., Antonellis, K.J., Scherf, U., Speed, T.P., 2003. Exploration, normalization, and summaries of high density oligonucleotide array probe level data. Biostatistics 4, 249-264.

Ji, J., Lee, H., Argiropoulos, B., Dorrani, N., Mann, J., Martinez-Agosto, J.A., Gomez-Ospina, N., Gallant, N., Bernstein, J.A., Hudgins, L.*, et al.*, 2015. DYRK1A haploinsufficiency causes a new recognizable syndrome with microcephaly, intellectual disability, speech impairment, and distinct facies. Eur J Hum Genet 23, 1473-1481.

Kannan, N., Neuwald, A.F., 2004. Evolutionary constraints associated with functional specificity of the CMGC protein kinases MAPK, CDK, GSK, SRPK, DYRK, and CK2alpha. Protein Sci 13, 2059-2077.

Kornev, A.P., Haste, N.M., Taylor, S.S., Eyck, L.F., 2006. Surface comparison of active and inactive protein kinases identifies a conserved activation mechanism. Proc Natl Acad Sci U S A 103, 17783-17788.

Kornev, A.P., Taylor, S.S., Ten Eyck, L.F., 2008. A helix scaffold for the assembly of active protein kinases. Proc Natl Acad Sci U S A 105, 14377-14382.

Kuleshov, M.V., Jones, M.R., Rouillard, A.D., Fernandez, N.F., Duan, Q., Wang, Z., Koplev, S., Jenkins, S.L., Jagodnik, K.M., Lachmann, A.*, et al.*, 2016. Enrichr: a comprehensive gene set enrichment analysis web server 2016 update. Nucleic Acids Res 44, W90-97.

Landrum, M.J., Lee, J.M., Benson, M., Brown, G., Chao, C., Chitipiralla, S., Gu, B., Hart, J., Hoffman, D., Hoover, J.*, et al.*, 2016. ClinVar: public archive of interpretations of clinically relevant variants. Nucleic Acids Res 44, D862-868.

Lin, C.W., Hsueh, Y.P., 2014. Sarm1, a neuronal inflammatory regulator, controls social interaction, associative memory and cognitive flexibility in mice. Brain Behav Immun 37, 142-151.

Mudunuri, U., Che, A., Yi, M., Stephens, R.M., 2009. bioDBnet: the biological database network. Bioinformatics 25, 555-556.

Najas, S., Arranz, J., Lochhead, P.A., Ashford, A.L., Oxley, D., Delabar, J.M., Cook, S.J., Barallobre, M.J., Arbones, M.L., 2015. DYRK1A-mediated Cyclin D1

degradation in neural stem cells contributes to the neurogenic cortical defects in Down syndrome. EBioMedicine 2, 120-134.

O'Roak, B.J., Vives, L., Fu, W., Egertson, J.D., Stanaway, I.B., Phelps, I.G., Carvill, G., Kumar, A., Lee, C., Ankenman, K.*, et al.*, 2012. Multiplex targeted sequencing identifies recurrently mutated genes in autism spectrum disorders. Science 338, 1619-1622.

Paxinos, G., Franklin, K.B.J. (2001). The mouse brain in stereotaxic coordinates, Second edition edn (San Diego, CA.).

Pfaffl, M.W., 2001. A new mathematical model for relative quantification in real-time RT-PCR. Nucleic Acids Res 29, e45.

Posey, J.E., Rosenfeld, J.A., James, R.A., Bainbridge, M., Niu, Z., Wang, X., Dhar, S., Wiszniewski, W., Akdemir, Z.H., Gambin, T.*, et al.*, 2016. Molecular diagnostic experience of whole-exome sequencing in adult patients. Genet Med 18, 678-685.

Ruaud, L., Mignot, C., Guet, A., Ohl, C., Nava, C., Heron, D., Keren, B., Depienne, C., Benoit, V., Maystadt, I.*, et al.*, 2015. DYRK1A mutations in two unrelated patients. Eur J Med Genet 58, 168-174.

Rump, P., Jazayeri, O., van Dijk-Bos, K.K., Johansson, L.F., van Essen, A.J., Verheij, J.B., Veenstra-Knol, H.E., Redeker, E.J., Mannens, M.M., Swertz, M.A.*, et al.*, 2016. Whole-exome sequencing is a powerful approach for establishing the etiological diagnosis in patients with intellectual disability and microcephaly. BMC Med Genomics 9, 7.

Smyth, G.K., 2004. Linear models and empirical bayes methods for assessing differential expression in microarray experiments. Stat Appl Genet Mol Biol 3, Article3.

Stessman, H.A., Xiong, B., Coe, B.P., Wang, T., Hoekzema, K., Fenckova, M., Kvarnung, M., Gerdts, J., Trinh, S., Cosemans, N.*, et al.*, 2017. Targeted

sequencing identifies 91 neurodevelopmental-disorder risk genes with autism and developmental-disability biases. Nat Genet 49, 515-526.

Tan, C.M., Chen, E.Y., Dannenfelser, R., Clark, N.R., Ma'ayan, A., 2013. Network2Canvas: network visualization on a canvas with enrichment analysis. Bioinformatics 29, 1872-1878.

Taylor, S.S., Kornev, A.P., 2011. Protein kinases: evolution of dynamic regulatory proteins. Trends Biochem Sci 36, 65-77.

Thomas, A., Burant, A., Bui, N., Graham, D., Yuva-Paylor, L.A., Paylor, R., 2009. Marble burying reflects a repetitive and perseverative behavior more than novelty-induced anxiety. Psychopharmacology (Berl) 204, 361-373.

Trujillano, D., Bertoli-Avella, A.M., Kumar Kandaswamy, K., Weiss, M.E., Koster, J., Marais, A., Paknia, O., Schroder, R., Garcia-Aznar, J.M., Werber, M.*, et al.*, 2017. Clinical exome sequencing: results from 2819 samples reflecting 1000 families. Eur J Hum Genet 25, 176-182.

Wang, T., Guo, H., Xiong, B., Stessman, H.A., Wu, H., Coe, B.P., Turner, T.N., Liu, Y., Zhao, W., Hoekzema, K.*, et al.*, 2016. De novo genic mutations among a Chinese autism spectrum disorder cohort. Nat Commun 7, 13316.

Zhang, Y., Kong, W., Gao, Y., Liu, X., Gao, K., Xie, H., Wu, Y., Zhang, Y., Wang, J., Gao, F.*, et al.*, 2015. Gene mutation analysis in 253 Chinese children with unexplained epilepsy and intellectual/developmental disabilities. PLoS One 10, e0141782.

Supplementary Table 1. Mutations analyzed in this study

Mutation	Codon change[a]	Position[b]	Reference	Clinical traits	ClinVar[h]	dbSNP[i]
K167R	A***A***A>A***G***A	β-sheet 1	De Rubeis et al., 2014	No information	-	rs1456204748
K188I	A***A***A>A***T***A	AX**K**-motif[c], β-sheet 3	Ji et al., 2015	IUGR; seizures; microcephaly; short stature; ID; global DD; broad-based gait; minor skeletal abnormalities; severe speech delay; distinct facial gestalt	SCV000206791	rs797044524
A195T	***G***CT>***A***CT	α-helix C	Dang et al., 2018	global DD; problems in social interaction; anxiety; repetitive behaviors; mild ID with particular impairments in language; infantile spams; complex partial epilepsy with epileptic encephalopathy	-	-
L207P	C***T***T>C***C***T	α-helix C, R-spine[d]	DDD et al., 2015	IUGR; global DD; microcephaly; delayed speech and language development; cleft soft palate; abnormality of the skeletal system; abnormality of the palmar creases; amblyopia; astigmatism	-	-
H223R	C***A***T>C***G***T	β-sheet 4	-	No information	SCV000620751	rs1555984071
L245R	C***T***C>C***G***C	α-helix D, C-spine[e]	Ji et al,. 2015	IUGR; global DD; ID; microcephaly; feeding difficulties in infancy; dysmorphic features; severe speech delay; brain abnormalities/MRI; skeletal anomalies; abnormal gait/ataxia; hand stereotypies; left renal agenesis	SCV000206792 SCV000807304	rs797044525
L259F	TT***G***>TT***T***	α-helix E	DDD et al., 2015; Dang et al., 2018	ASD/ID/DD and pervasive developmental disorder, not otherwise specified: extremely low cognitive abilities and adaptive functioning, consistent with the mild range of ID; anxiety, perseveration and additional upsets and aggressive behavior	-	-
A277P	***G***CG>***C***CG	α-helix E	DDD et al., 2015; Evers et al., 2017	global DD; postnatal microcephaly; decreased facial expression; hypoplastic left heart; micrognathia; retinal dystrophy	SCV000571206	rs1064795422
D287V	G***A***T>G***T***T	HC**D**-motif[f], R-spine	DDD et al., 2015	IUGR; microcephaly; feeding difficulties in infancy; early cataracts; short stature; specific learning disability; abnormality of the frontal hairline; single transverse palmar crease; cerebellar atrophy; ventriculomegaly; abnormality of the skin	-	rs1555984343
D287V	G***A***T>G***T***T	HC**D**-motif[f], R-spine	-	young patient with development delay, epilepsy and microcephaly, in combination with another variant in CPA6 (VUS)	SCV000598121	rs1555984343
D287Y	***G***AT>***T***AT	HC**D**-motif, R-spine	Zhang et al., 2015	severe ID/DD; generalized tonic-clonic seizures, febrile seizures, status epilepticus	-	-
L295F	***C***TT>***T***TT	β-sheet 7, C-spine	Ji et al., 2015	microcephaly; dysmorphic features; mild global DD; severe speech delay; skeletal anomalies; blepharophimosis; abnormal gait/ataxia	SCV000206793 SCV000321572	rs797044526
F308V	***T***TT>***G***TT	D**F**G-motif[g], R-spine	-	No information	SCV000247240	rs797045540
S311F	T***C***T>T***T***T	β-sheet 9	Ruaud et al., 2015	ID; small stature; epilepsy; recurrent infections; microcephaly	SCV000586742 SCV000520979	rs1039571136
Q313H	CA***G***>CA***T***	β-sheet 9	De Rubeis et al., 2014	No information	-	rs770863323
R325H	C***G***C>C***A***C	P+1 loop	-	No information	SCV000574147	rs1064796923

Y327C	T***A***T>T***G***T	P+1 loop	-	No information	SCV000599256	rs1555985554
R328W	***C***GG>***T***GG	P+1 loop	Stessman et al., 2017	No information	SCV000492371	rs113004433
S346F	T***C***C>T***T***C	α-helix F	-	No information	SCV000712522	rs1555985649
S346P	***T***CC>***C***CC	α-helix F	DDD et al., 2015	seizures; global DD; microcephaly	-	rs724159951
S346P	***T***CC>***C***CC	α-helix F	Bronicki et al., 2015	seizures; feeding difficulties in infancy; deeply set eye; microcephaly; ID; absent or delayed speech development; hypermetropia/ myopia; large/dysplastic ears; thin upper lip; micrognathia; prone to infections	SCV000196060	rs724159951
L347R	C***T***C>C***G***C	α-helix F	Trujillano et al., 2017	microcephaly; ID; seizures; spasticity; global DD; motor delay; hypertonia; abnormal facial shape; cortical dysplasia; cortical gyral simplification; short stature	-	-
R438H	C***G***T>C***A***T	CMGC-insert	Wang et al., 2016	No information	-	rs1379071994
R458M	A***G***G>A***T***G	α-helix H	Dang et al., 2018	No information	-	-
R467Q	C***G***A>C***A***A	N-terminal to α-helix I	Posey et al., 2016	developmental regression; ID; hypotonia; mild ataxia; intention tremor; dysmorphisms; primary microcephaly; failure to thrive; demyelination; sun sensitivity; incontinence and anxiety	SCV000245477 SCV000534701	rs797045041
R467Q	C***G***A>C***A***A	N-terminal to α-helix I	Decipher et al., 2015	micrognathia; low set ears; truncal obesity; facial asymmetry; lordotic posture with broad based gait; reduced muscle tone; feet brachydactyly with bilateral symmetrical 2-3 toe syndactyly; febrile convulsions in childhood- no seizures since; mild learning difficulties	-	rs797045041
R467*	***C***GA>***T***GA	N-terminal to α-helix I	Ji et al., 2015; Posey et al., 2016	feeding difficulties in infancy; dysmorphic features; global DD; severe speech delay; moderate ID; seizures; brain abnormalities/MRI; skeletal anomalies; astigmatism	SCV000206787 SCV000245476 SCV000618033	rs797044520
F478Sfs112*	AG***T*** TTC >AGT TCT	C-terminal to α-helix I	Rump et al., 2016	low birth weight; brachycephaly; hypertonia; severe DD	-	-
G486D	G***G***T>G***A***T	C-terminal to α-helix I	Dang et al., 2018	ASD, learning disorder and macrocephaly	SCV000747759	rs1555991030
A498Pfs93*	CCC G***C***C>CCC GCA	C-terminal to α-helix I	O'Roak et al., 2012	microcephaly; global DD; speech delay; febrile and febrile seizures; recurrent otitis media with myringotomy; urinary problems; strep throat; head circumference of 48 cm (z =-2.7) and normative BMI	SCV000056592 SCV000494645	rs1057519628
R528W	***C***GG>***T***GG	non-catalytic C-end	-	No information	SCV000594478	rs1448604709
T588N	A***C***C>A***A***C	non-catalytic C-end	Bronicki et al., 2015	seizures; feeding difficulties in infancy; deeply set eye; microcephaly; ID; absent or delayed speech development	SCV000196065	rs724159955

[a], the nucleotide change is shown in bold; [b], location of the amino acid change within the catalytic domain secondary structure; [c], motif within the β3 strand in which the lysine couples the phosphates of ATP to the α-helix C (Taylor and Kornev, 2011); [d], the R-spine or regulatory spine is a conserved spatial motif in active kinases (Kornev et al., 2006); [e], the C-spine or catalytic spine is a conserved hydrophobic spine within the catalytic core (Kornev et al., 2008); [f], key motif within the catalytic loop in which the central arginine has been replaced by a cysteine in the DYRK family of kinases alone (Kannan and Neuwald, 2004); [g], motif where aspartic acid is critical for recognizing one of the ATP-bound Mg^{2+} ions (Taylor and Kornev, 2011); [h], ClinVar: www.ncbi.nlm.nih.gov/clinvar (Landrum et al., 2016); [i], www.ncbi.nlm.nih.gov/variation/view.
ASD, autism spectrum disorder; BMI, body mass index; DD, developmental delay; ID, intellectual disability; IUGR, intrauterine growth retardation; MRI, magnetic resonance imaging.

Supplementary Table 2. Primers used for site directed mutagenesis

Name	Sequence (5' -> 3')[a]
K167R	AATTGACTCCTTGATAGGC**AGA**GGTTCCTTTGGACAGGTTG
K188I	GCAAGAATGGGTTGCCATT**ATA**ATAATAAAGAACAAGAAGG
A195T	AAATAATAAAGAACAAGAAG**ACT**TTTCTGAATCAAGCACAG
L207P	ACAGATAGAAGTGCGACTT**CCT**GAGCTCATGAACAAACATG
H223R	ATGAAATACTACATAGTG**CGT**TTGAAACGCCACTTTATG
L245R	GAAATGCTGTCCTACAAC**CGC**TATGACTTGCTGAGAAAC
L259F	AATTTCCGAGGGGTCTCT**TTT**AACCTAACACGAAAGTTTGCGC
A277P	GCACTGCACTGCTTTTCCTT**CCG**ACTCCAGAACTTAGTATC
D287V	ACTTAGTATCATTCACTGT**GTT**CTAAAACCTGAAAATATCC
D287Y	GAACTTAGTATCATTCACTGT**TAT**CTAAAACCTGAAAATATCC
L295F	TAAAACCTGAAAATATCCTT**TTT**TGTAACCCCAAACGCAG
F308V	GTGCAATCAAGATAGTTGAC**GTT**GGCAGTTCTTGTCAGTTGG
S311F	ATAGTTGACTTTGGCAGT**TTT**TGTCAGTTGGGGCAGAGG
Q313H	GACTTTGGCAGTTCTTGT**CAT**TTGGGGCAGAGGATATACC
R325H	CTCTGGAGACCGATAAAA**GTG**ACTCTGAATATACTGGTA[b]
Y327C	GTATATTCAGAGTCGCTTT**TGT**CGGTCTCCAGAGGTGCTAC
R328W	ATATTCAGAGTCGCTTTTAT**TGG**TCTCCAGAGGTGCTACTG
S346P	CCTTGCCATTGATATGTGG**CCC**CTCGGGTGTATTTTGG
S346F	CCTTGCCATTGATATGTGG**TTC**CTCGGGTGTATTTTGG
L347R	TTTCAACCAAAATACACCC**GCG**GGACCACATATCAATGGC[b]
R438H	ATGACCTGACTCCCCAGC**ATG**TCGCCCACCAGGTCCTCC[b]
R458M	TTCAAAGACCTCATTTTA**ATG**ATGCTTGATTATGACCCC
R467*	GATTATGACCCCAAAACT**TGA**ATTCAACCTTATTATGC
R467Q	TGATTATGACCCCAAAACT**CAA**ATTCAACCTTATTATGC
F478Sfs112*	TTATGCTCTGCAGCAC**AGTTC**TTCAAGAAAACAGCTGATG[c]
G486D	CAAGAAAACAGCTGATGAA**GAT**ACAAATACAAGTAATAGTG
A498Pfs93*	TAGTGTATCTACAAGC**CCCGC**ATGGAGCAGTCTCAGTC[d]
R528W	CAAGCAACAGTGGGAGAGCC**TGG**TCGGATCCGACGCACCAG
T588N	CATCCTGTTCAAGAAACA**AAC**TTTCATGTAGCCCCTCAAC

[a], mutated codon is shown in bold; [b], reverse complement; [c], T deletion; [d], C deletion.

Supplementary Table 3. Primary antibodies used for immunoblotting

Antibody	Host	Source	Dilution
DYRK1A	Mouse	Abnova (H000001859)	1/1000
DYRK1A	Rabbit	Abcam (ab69811)	1/1000
GFP	Mouse	Clontech (632381)	1/2000
HA	Mouse	Covance (MMS-101R)	1/2000
phospho-Tyr (PY99)	Mouse	Santa Cruz (sc-7020)	1/1000
α-Tubulin	Mouse	Sigma (T6199)	1/5000

Supplementary Table 4. Primers used for qPCR

Gene symbol	Sequence (5’ -> 3’; forward)	Sequence (5’ -> 3’; reverse)
Dyrk1a	ATCCAGCAACTGCTCCTCTG	CCGCTCCTTCTTATGACTGG
Htr7	CCCTGAAACTTGCTGAGAGG	CCAATGGTTTCGTTGTTTCC
Nefl	GAGCGAGATGGCCAGGTA	TCTGAGAGTAGCCGCTGGTT
Nefm	ACAACCACGACCTCAGCAG	TGGTATTCTCGCAAATGACG
Nfi1b	CGCATGGAGTCACTATTCCTG	ATAAAATGGCTGGCTATGG
Penk	AGCCAGGACTGCGCTAAAT	GCAGGTCTCCCAGATTTTGA
Ppia	ATGGCAAGACCAGCAAGAAG	TTACAGGACATTGCGAGCAG

Supplementary Table 5. Probes used in the Low Density Array

Gene Symbol	Assay ID	Gene Symbol	Assay ID
Actb	Mm00607939_s1	*Nfib*	Mm00500784_m1
Aplp2	Mm00507819_m1	*Notch2*	Mm00803077_m1
Aqp4	Mm00802131_m1	*Nrn1*	Mm00467844_m1
B3gnt1	Mm00723578_m1	*Olfm3*	Mm00462529_m1
Chn1	Mm00472572_m1	*Ppia*	Mm02342429_g1
Cnp1	Mm00487038_m1	*Ptger4*	Mm00436053_m1
Ddit4	Mm00512503_g1	*Rab27b*	Mm00472653_m1
Gabarapl1	Mm00457880_m1	*S100b*	Mm00485897_m1
Gabrb3	Mm00433473_m1	*Slc32a1*	Mm00494138_m1
Gabrg1	Mm00439047_m1	*Sox11*	Mm03053654_s1
Gfap	Mm00546086_m1	*Sox4*	Mm00486320_s1
Got1	Mm00494693_m1	*Sst*	Mm00436671_m1
Gpr6	Mm01701705_s1	*Syt11*	Mm00444517_m1
Htr7	Mm00434133_m1	*Thy1*	Mm00493681_m1
Itsn1	Mm00495015_m1	*Tspan17*	Mm00512218_m1
Kifc2	Mm00495166_g1	*Tspan2*	Mm00510514_m1
Lin7b	Mm00457059_m1	*Tuba4a*	Mm00849767_s1
Mbp	Mm01262035_m1	*Unc13c*	Mm00463432_m1
Myrip	Mm00460563_m1	*Vsnl1*	Mm00449558_m1

Supplementary Table 6. Primary antibodies used for immunostaining

Antibody	Host	Source	Dilution
BrdU	Rat	Serotec (OBT0030G)	1:100
Ctip2*	Rat	Abcam (ab18465)	1:250
GABA	Rabbit	Sigma-Aldrich (A2052)	1:200
Gephyrin*	Mouse	Synaptic Systems (147 011)	1:500
Homer*	Mouse	Thermo Scientific (MA1-045)	1:1000
Mef2c*	Rabbit	Abcam (ab64644)	1:250
NeuN	Mouse	Chemicon (MAB377)	1:1000
VGAT*	Rabbit	Synaptic Systems (131 003)	1:400
VGlut1*	Guinea-pig	Milipore (AB5905)	1:700

*Citrate pretreatment

Supplementary Figure Legends

Supplementary Fig. 1. Biochemical analysis of *DYRK1A* mutants.
(A) Analysis of the autophosphorylation activity of the DYRK1A mutants shown in Fig. 1. The graphs show the mean ± SEM, with the WT values set arbitrarily as 100 (n=3). In the authophosphorylation assays in A and B, nd refers to radioactive signals at the background level (ns= not significant, *$p < 0.05$, **$p < 0.01$, ***$p < 0.001$, unpaired 2-tailed Mann-Whitney's test). (B) Representative images of the autophosphorylation assays for selected DYRK1A mutants. (C) Accumulation of DYRK1A mutants calculated as described in Fig. 1E, with the WT protein values set arbitrarily as 100 (mean ± SEM, n=3 independent experiments; ns= not significant, **$p < 0.01$, ***$p < 0.001$, unpaired 2-tailed Mann-Whitney's test).

Supplementary Fig. 2. Ultrasonic vocalization and duration of social contacts.
(A) Number and duration of UsV calls recorded over 5 min from pups when separated from their mothers at the developmental stage indicated (*Dyrk1a*$^{+/+}$, n=17; *Dyrk1a*$^{+/-}$, n=11). UsV data was analyzed by two-way ANOVA followed by a Bonferroni post-hoc test. The differences between the genotypes were statistically significant: $F_{(1.94)}=13.25$, p = 0.0004 (number of calls) and $F_{(1.92)} =40.92$, $p < 0.0001$ (call duration), two-way ANOVA. Differences in call duration were significant in the Bonferroni post-hoc test (*$p < 0.05$, **$p < 0.01$). (B) Social contacts (sniffing) performed by *Dyrk1a*$^{+/+}$ and *Dyrk1a*$^{+/-}$ mice in the social interaction test. The graph represents the number of sniffs (mean ± SEM) over 5 min distributed according to their duration (*X*-axis correspond to seconds). Note that *Dyrk1a*$^{+/-}$ mice engaged in significantly fewer social contacts longer than 6 s: (n=12-15 mice each genotype; *$p < 0.05$, **$p < 0.01$, Student's *t*-test).

Supplementary Fig. 3. Scheme showing the workflow for the automatic quantification of synapses from confocal images using an image-processing algorithm written in Fiji macro language.

(A) The macro opens a raw data image from a folder of choice (file with an extension *.lsm). (B) The algorithm splits the channels and normalizes their names to “Blue” (DAPI nuclear staining), “Green” (Alexa Fluor-488 for post-synaptic labeling of Homer or Gephyrin) and “Red” (Alexa Fluor-568 for pre-synaptic labeling of VgluT1 or VGAT). As Gephyrin (example in panel B) but not Homer is found in the nuclei, there were minor differences in the processing of the “Green” signal in some of the following steps. (C) The “Blue” channel is pre-processed to remove the noise by applying a Gaussian filter (Radius=2) and a Rolling Ball algorithm (Radius=80). An automatic threshold (Li) was then applied and the objects were filtered to generate a binary mask containing only the nuclei. In the case of Gephyrin^{+}/VGAT^{+} images, the “Green” channel was pre-processed with a Gaussian filter (Radius=5), automatically thresholded (Huang) and the objects were filtered to generate a second mask containing only the nuclei. Both masks (Gephyrin and DAPI nuclear signals) were combined to obtain a single nuclear mask. (D) The inverted nuclear mask defines the working area, and this value was stored and used in the final calculation of synapse density, the selected area being used to estimate the median signal value of the “Red” channel. The median signal values for all the images in the data set were averaged to obtain a global median value, which was used at a later step as a reference to normalize the red channel. (E) To enhance spot discrimination, the original “Green” channel was filtered using the Laplacian of Gaussian (Radius=2) operator. After applying an automatic threshold (Otsu), the spots detected were filtered according to size (0.01-100 μm^2) and circularity criteria (0.6-1), and used to produce a binary mask. Finally, the watershed algorithm was used to further separate contiguous particles. (F) The segmented post-synaptic particles in the original “Green” channel were further filtered according to the density of their

intensity, and small and/or weak particles below a certain threshold were discriminated. (G) To count synapses, the “Red” channel was first translated to correct for the chromatic shift (x=0.87 and y=1.31: values calculated using fluorescent microspheres), it was pre-processed with a Median filter (Radius=2) and Rolling ball algorithm (Radius=120) to remove noise, and it was normalized by the global median signal calculated in D. The macro counts a synapse as every green particle selected that overlies at least one pixel with a relevant intensity in the red channel. A verification image is then generated that contains all three processed channels and the synapse events highlighted in white. (H) The macro analyses all the images included in a folder of choice and delivers a text file for each image that contains the image name, the median red intensity value, the working area value, the number of segmented green particles, the number of filtered green particles and the number of synapses. Synapse density was calculated by dividing the number of synapses by the value of the working area.

Supplementary Fig. 4. Neuron production in the dorsal telencephalon of E17.5 *Dyrk1a*$^{+/+}$ and *Dyrk1a*$^{+/-}$ embryos.

(A) Schedule of the BrdU-labeling protocol to estimate neuron production in the developing neocortex. (B) Representative images of the SSC of P7 *Dyrk1a*$^{+/+}$ and *Dyrk1a*$^{+/-}$ animals showing BrdU^{+} cells immunopositive for the neuronal marker NeuN (arrowheads). Bar = 50 μm. The histogram represents the number of BrdU^{+}/NeuN^{+} neurons in a 500 μm wide column of the neocortex (n=3 animals each genotype; ns=not significant, Student’s *t*-test). In both genotypes, the are few BrdU^{+}/NeuN^{+} neurons and these neurons are positioned in the most external part of the neocortex.

Supplementary Fig. 5. Dyrk1a expression in the developing cerebral cortex of *Dyrk1a*$^{+/-}$ mutants and their WT littermates.

(A) *Dyrk1a* mRNA in the developing cerebral cortex of *Dyrk1a*$^{+/+}$ and *Dyrk1a*$^{+/-}$ embryos or postnatal animals. The graph represents the mRNA expression relative to the levels in E11.5 *Dyrk1a*$^{+/+}$ embryos set arbitrarily as 1 (n ≥ 3; $^{**}p < 0.01$, Student's *t*-test, +/- vs +/+ at any time point). Note that the reduced *Dyrk1a* expression in the mutants is maintained during embryonic and postnatal development. (B, C) Representative Western blots of extracts prepared from P0 (B) and P7 (C) cerebral cortices and probed with the antibodies indicated. The secondary antibody was detected by infrared fluorescence using the LI-COR Odyssey IR Imaging System V3.0 (LI-COR Biosciences, Cambridge, UK). The graphs represent the Dyrk1a protein normalized to Vinculin levels and expressed relative to the WT animals. Note that there is approx. 50% less Dyrk1a in *Dyrk1a*$^{+/-}$ mice (n=3 mice each genotype): $^{**}p < 0.01$, Student's *t*-test.

Supplementary Fig. 6. Gene expression in the postnatal *Dyrk1a*$^{+/+}$ and *Dyrk1a*$^{+/-}$ cerebral cortex.

(A) Experimental design indicating the animal number (#1 or #2), the genotype (*Dyrk1a*$^{+/+}$, +/+; *Dyrk1a*$^{+/-}$, +/-) and the litter (litters 2 and 3 for P0 samples and litters 1 and 4 for P7 samples) used in the Affymetrix array. Experiment (Exp.) 1 and 2 refers to the number of the array cartridge used for hybridization. Two samples for each experimental condition (developmental stage, genotype and litter) were included in each cartridge. (B) Heatmap showing gene expression in WT (*+/+) and Dyrk1a* mutant (+/-) samples at P0 and P7. The rows represent the individual probes and the values in the color-coded scale bar correspond to the standard deviation of each probe from the log2 mean expression value. The differences between the genotypes are smaller than between the developmental stages and they were more evident at P0 than at P7. Note that inter- and intra-litter variability is similar.

Supplementary Fig. 7. qPCR validation of the microarray data from a low-density array (LDA).

Experimental details for the LDA are described in the Supplementary Materials and Methods, and the probes used are listed in Table 5. We selected a set of 36 genes that show the difference in expression between P7 and P0 in the WT (*Dyrk1a*$^{+/+}$) samples on the Affymetrix array (adjusted *p*-value < 0.05). The qPCRs were performed in samples obtained from P0 and P7 *Dyrk1a*$^{+/+}$ and *Dyrk1a*$^{+/-}$ animals (n=4 animals of each genotype and developmental stage). The graphs represent the mean log2 fold-change in value of each gene obtained in the Affymetrix (black bars) and the LDA array (grey bars). Correlation of the log2 fold-change from the microarray and LDA results was calculated with a Pearson's correlation test. The array and LDA results showed significant correlations in both *Dyrk1a*$^{+/+}$ and *Dyrk1a*$^{+/-}$ samples. The changes in mRNA expression were consistent (up- or down-regulated at P7) through the two experimental approaches, with the exception of *Aplp2* in the *Dyrk1a*$^{+/+}$ samples and *Ddit4* in the *Dyrk1a*$^{+/-}$ samples. The dotted lines indicate the log2 fold-changes equal to ±0.4.

Supplementary Fig. 8. Pathway enrichment analysis of the transcriptome data in *Dyrk1a*$^{+/+}$ cortices during development (P7 vs P0).

Enrichment terms for the up-regulated and down-regulated genes at P7 relative to the P0 cortices of WT animals, determined using the Enrichr gene set enrichment analysis and visualization tools. The enriched terms are highlighted in color where the brightness indicates a lower *p*-value. Selective relevant enriched terms are listed on the side on the canvas (ChEA, published ChIP-sequencing data sets; KEGG, cellular and molecular pathways database; MGI-MP, mammalian phenotypes from the Mouse Genome Informatics: see Supplementary Dataset 2 for a complete list of enriched terms). The CHEA analysis indicated that the up-regulated genes were

enriched in Polycomb targets, whereas the down-regulated gene set was enriched in targets of the proliferation-associated transcription factor FOXM1. Note that the enrichment analysis of the mammalian phenotype ontology revealed terms like abnormal synaptic transmission, seizures and abnormal learning in the up-regulated gene set, and abnormal nervous system in the down-regulated set.

Supplementary Movie. Example of a generalized tonic-clonic (GTC) seizure recorded in a *Dyrk1a*$^{+/-}$ mouse. The first manifestation of a GTC seizure is a typical Straub reaction, consisting of a rigid and erected tail lying across the back of the animal in an S-shaped curve. This reaction is followed by facial jerks, myoclonus, the mouse falling on its side and irregular twitches with hyperextension of the limbs, which evolves into a clonic stage with wild jumping and tonic hind-limb extension, and an after-seizure period of immobility. The onset of the GTC seizure is missed in the video-EEG because it occurred while connecting the mouse electrodes to the equipment after placing the mouse in the video-EEG cage.

Supplementary Figure 1
Arranz *et al.*

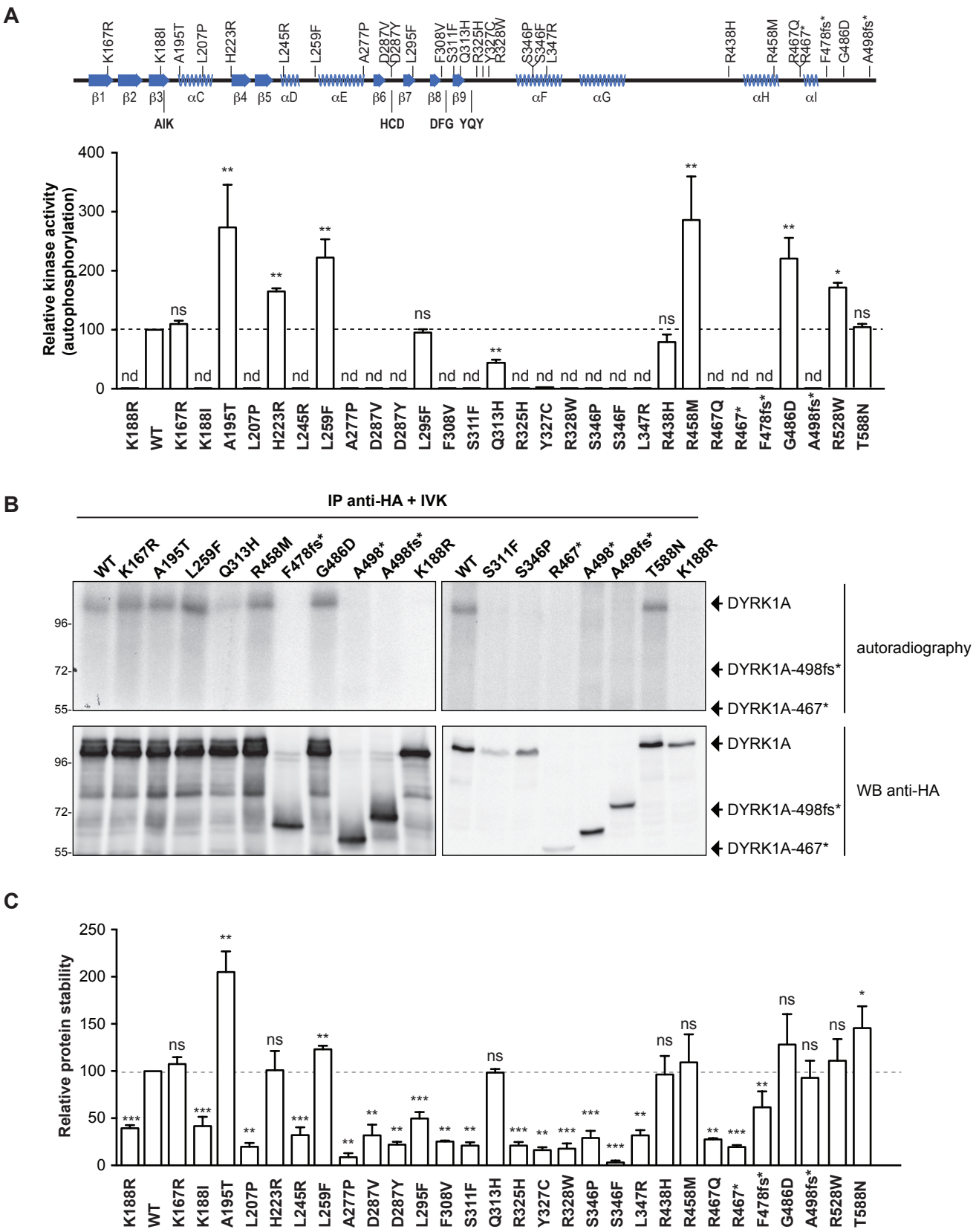

Supplementary Figure 2
Arranz *et al.*

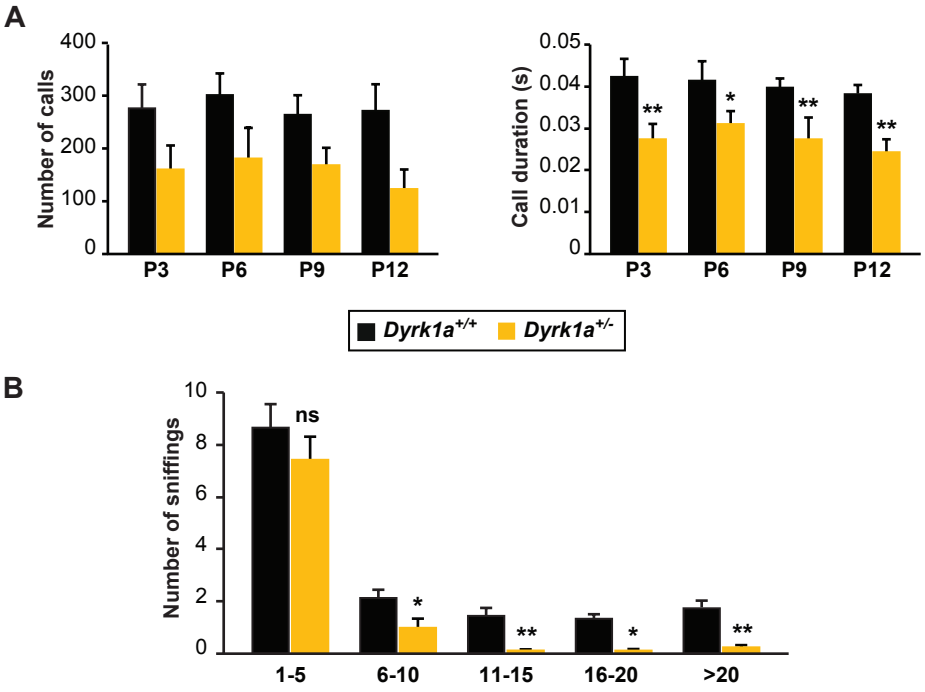

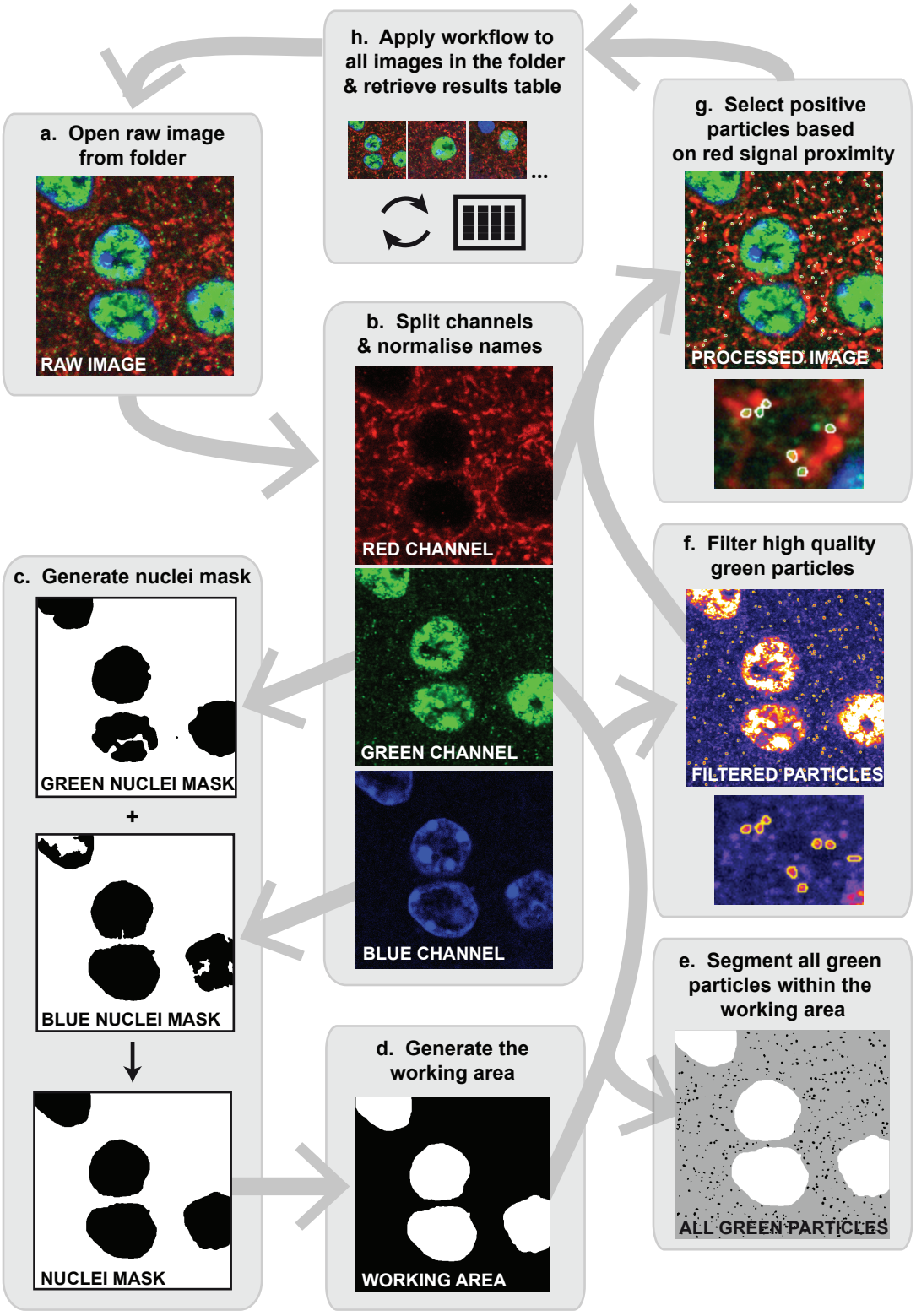
h. Apply workflow to all images in the folder & retrieve results table
...
a. Open raw image from folder
RAW IMAGE
b. Split channels & normalise names
RED CHANNEL
GREEN CHANNEL
BLUE CHANNEL
g. Select positive particles based on red signal proximity
PROCESSED IMAGE
f. Filter high quality green particles
FILTERED PARTICLES
c. Generate nuclei mask
GREEN NUCLEI MASK
+
BLUE NUCLEI MASK
NUCLEI MASK
d. Generate the working area
WORKING AREA
e. Segment all green particles within the working area
ALL GREEN PARTICLES

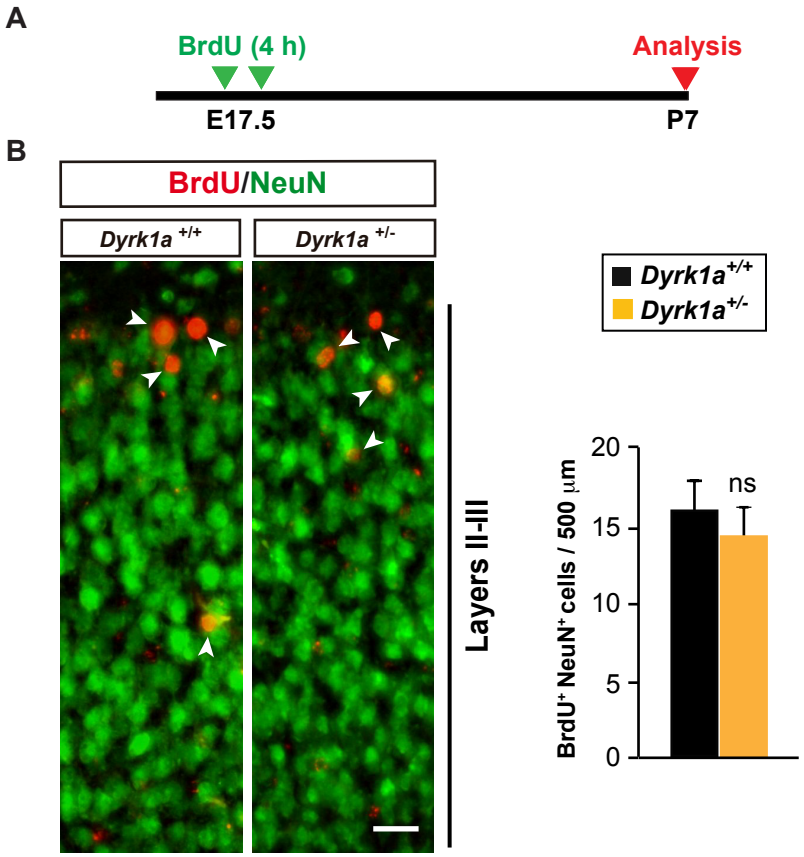
A
BrdU (4 h)
Analysis
E17.5
P7
B
BrdU/NeuN
Dyrk1a +/+
Dyrk1a +/-
Layers II-III
Dyrk1a+/+
Dyrk1a+/-
BrdU+ NeuN+ cells / 500 μm
20
15
10
5
0
ns

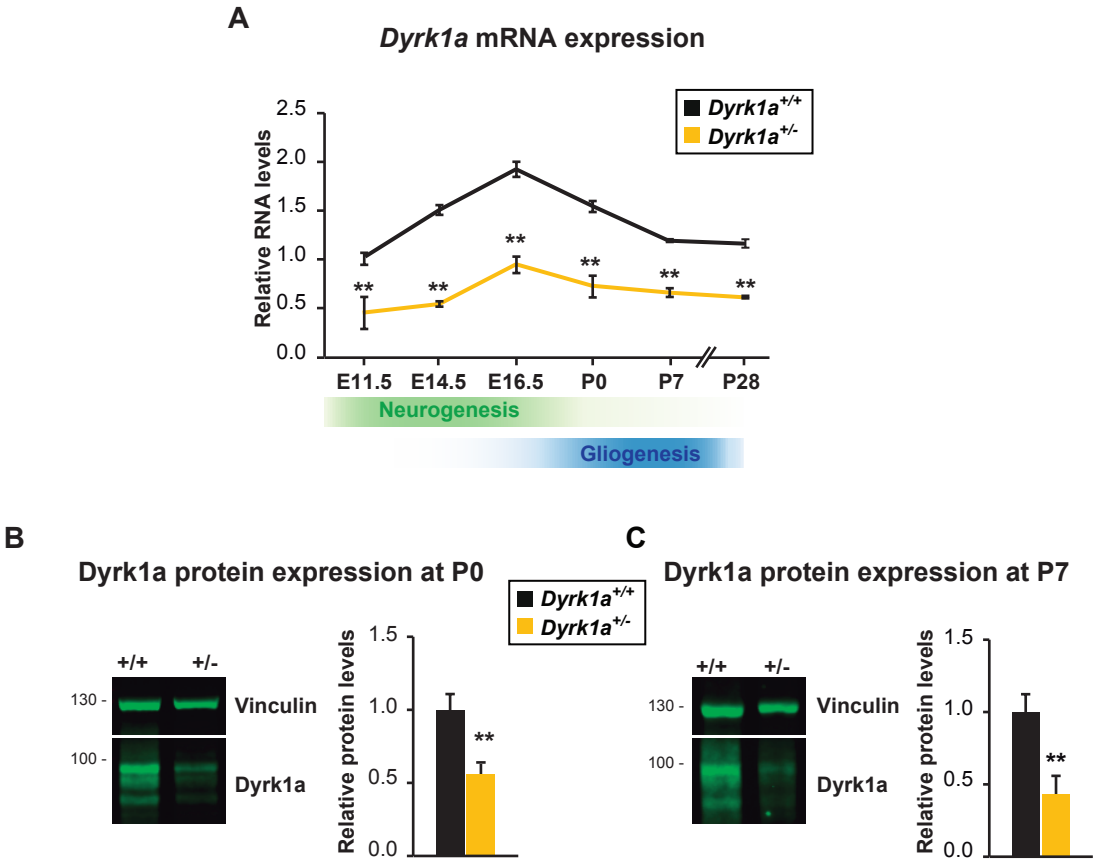
A
Dyrk1a mRNA expression
Dyrk1a+/+
Dyrk1a+/-
Relative RNA levels
2.5
2.0
1.5
1.0
0.5
0.0
**
E11.5
E14.5
E16.5
P0
P7
P28
Neurogenesis
Gliogenesis
B
Dyrk1a protein expression at P0
+/+
+/-
130 -
100 -
Vinculin
Dyrk1a
Relative protein levels
C
Dyrk1a protein expression at P7

Supplementary Figure 6
Arranz *et al.*

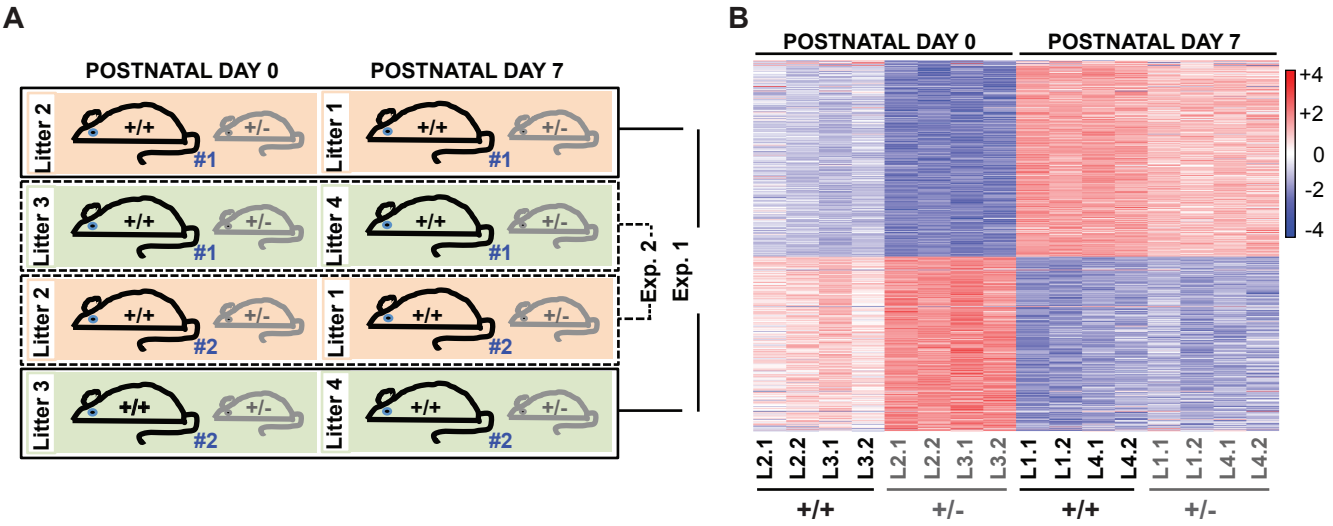

Supplementary Figure 7
Arranz *et al.*

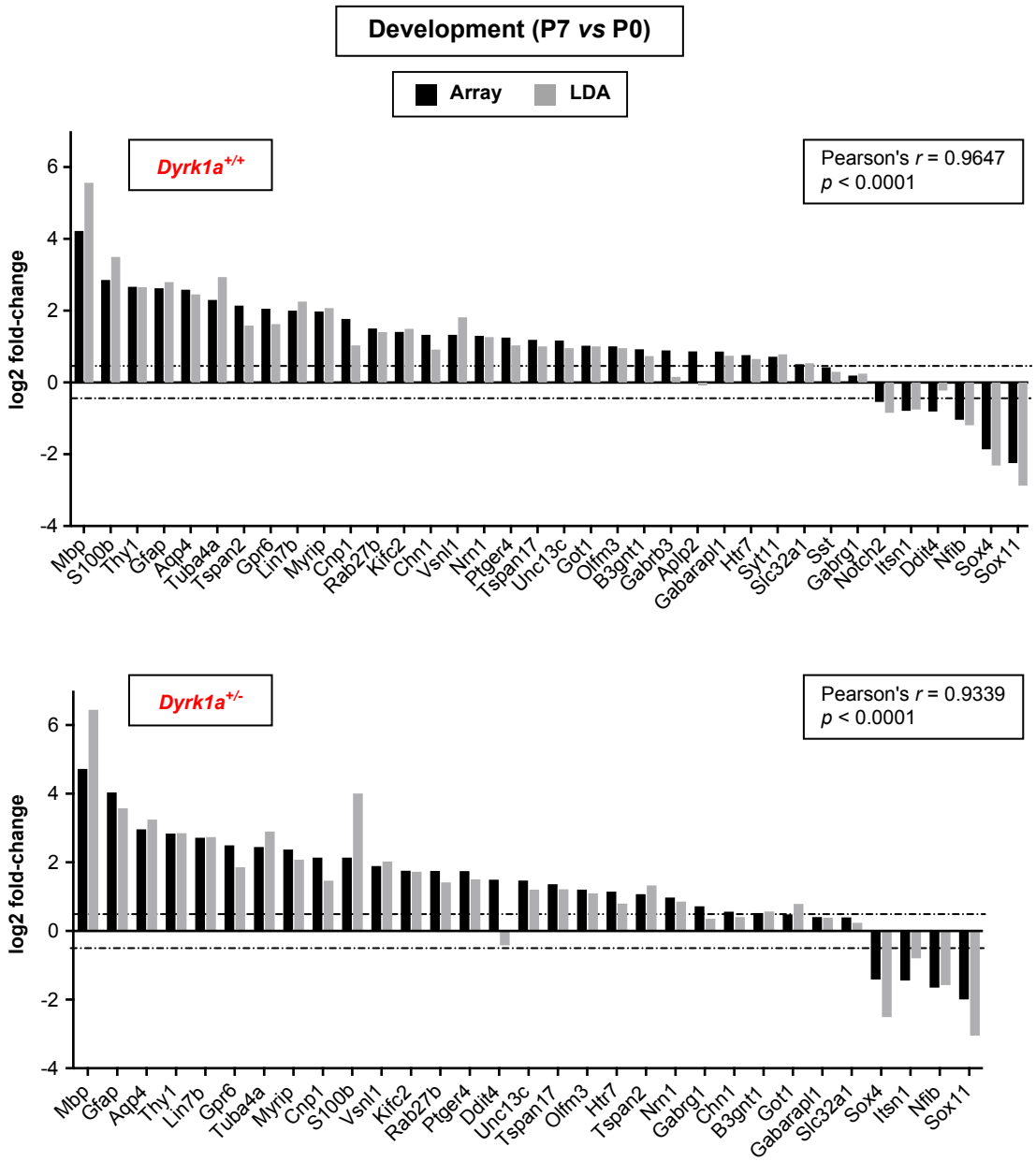

Supplementary Figure 8
Arranz *et al.*